EES Solar

COMMUNICATION

View Article Online
View Journal

Cite this: DOI: 10.1039/d6el00069j

Received 17th April 2026
Accepted 29th May 2026

DOI: 10.1039/d6el00069j

rsc.li/EESSolar

Probing encapsulation-induced changes in 2D/3D perovskite heterostructures for perovskite solar cells

Xin Liu,†[a] Tai Wu,†[b] Jingwen Cao,[b] Xiaoran Sun,[a] Meng Zhang *[ab] and Xiaojing Hao*[b]

Two-dimensional/three-dimensional (2D/3D) perovskite heterostructures have been extensively employed for effective interfacial defect passivation, enabling highly efficient perovskite solar cells (PSCs). At the same time, encapsulation plays a vital role in ensuring the long-term stability of PSCs toward commercialization. However, conventional lamination-based encapsulation processes involve elevated temperatures and mechanical pressure, and the resulting thermal and mechanical stress on the 2D/3D heterostructure within the device remains largely underexplored. Herein, we investigated how encapsulation affects 2D/3D perovskite heterostructures by probing the photoluminescence properties of films before and after encapsulation. In particular, we compare encapsulation effects for (100)- and (111)-oriented perovskites using various 2D passivants to form 2D/3D heterostructures. The results suggest that encapsulation-induced degradation in 2D/3D heterostructures based on conventional mixed-oriented perovskites primarily originates from those formed on (100)-oriented perovskites, whereas those on (111)-oriented perovskites are more tolerant to the thermal lamination conditions used during encapsulation. This work provides critical insights into perovskite structural evolution during the encapsulation process, advancing their path toward stable commercial applications.

Broader context

2D/3D perovskite heterostructures are widely used to passivate interfaces and boost the efficiency of perovskite solar cells, yet their robustness under industrial encapsulation conditions is rarely considered. Practical encapsulation involves heat and mechanical pressure, which can introduce substantial stress to perovskite layers and compromise device stability. This work shows that the crystallographic orientation of the perovskite critically influences the encapsulation tolerance of 2D/3D heterostructures, with (111)-oriented perovskites exhibiting markedly higher resilience than their conventional (100)-oriented counterparts. By linking interface design with encapsulation-induced structural evolution, these findings provide a concise design guideline for developing perovskite solar cells that combine high efficiency with the durability required for commercial deployment.

1 Introduction

Perovskite photovoltaics (PVs) have emerged as one of the most promising candidates for next-generation solar technologies owing to their outstanding power conversion efficiency (PCE, over 27%),[1] facile and low-cost manufacturing processes, tuneable bandgaps, mechanical adaptability, and, notably, recent improvement in long-term operational stability, which are bringing them increasingly closer to commercial viability.[2–5] The performance-boosting effect of two-dimensional (2D) passivation on perovskite solar cells (PSCs) is evident, with organic salts such as phenethylammonium iodide (PEAI) and octylammonium iodide (OAI) being commonly employed as passivating agents.[6–8] For example, a study reports that PEAI forms a 2D layer on the 3D perovskite surface, which passivates defects and suppresses non-radiative recombination, resulting in record level efficiency.[9] Although the 2D/3D perovskite heterostructure can combine the superior environmental stability of a 2D perovskite with the high optoelectronic performance of a 3D perovskite, recent studies have revealed that 2D perovskite films are not composed of a homogeneous phase. Instead, they consist of vertically stacked phases with varying layer numbers (n = 1, 2, 3, …).[8,10] The resulting films exhibit uncontrolled phase composition and thickness, with poorly defined n-values.[11] Furthermore, studies show that conventional spacer cations often struggle to form stable 2D layers on inorganic perovskites because they cannot replace tightly bound Cs^+ ions. Under heat, these cations tend to diffuse into the 3D lattice, which negatively affects the structural and electronic properties of the perovskite, ultimately reducing device performance.[12,13] These findings reveal that the 2D/3D

[a]School of New Energy and Materials, Southwest Petroleum University, Chengdu 610500, People's Republic of China

[b]The Australian Centre for Advanced Photovoltaics, School of Photovoltaic and Renewable Energy Engineering, University of New South Wales, Sydney, NSW 2052, Australia. E-mail: xj.hao@unsw.edu.au; meng.zhang@unsw.edu.au

† These authors contributed equally to this work.

interface is not inherently stable, which can potentially be more pronounced under external stresses, such as stresses induced in the encapsulation process.

Encapsulation is indispensable for the commercialization of perovskite photovoltaics, as it protects the device from moisture and oxygen ingress and mechanical damage.[14] However, while the stabilizing role of encapsulation is well established, its impact on the structural integrity and interfacial dynamics of 2D/3D perovskite heterostructures remains insufficiently understood, largely because de-encapsulation is experimentally challenging and, even when feasible, the process itself may induce film damage. Existing encapsulation studies have primarily focused on the selection of encapsulant materials, such as polyisobutylene (PIB) and ethylene-vinyl acetate (EVA), and the development of strategies to improve long-term device reliability.[15–17] Despite these advances, the potential impact of the encapsulation process itself has been largely overlooked, especially the thermal, mechanical, and chemical stresses associated with lamination or curing, which can compromise interfacial stability and trigger phase transitions, ionic redistribution, or interlayer decoupling in 2D/3D perovskite heterostructures. Additionally, most of the encapsulation strategies employ lamination-based processes developed from silicon solar cell encapsulation. The lamination process typically involves external factors such as elevated temperatures and mechanical pressure.[18] While these external stimuli exert minimal influence on stable silicon solar cells, they warrant careful consideration in the context of the comparatively sensitive PSCs.[19,20]

In this regard, we introduce a pre-inserted spacer layer prior to encapsulation,[17] which facilitates subsequent de-encapsulation without compromising sample integrity and thereby enables systematic elucidation of the thermal-lamination impact on 2D/3D perovskite heterostructures formed with PEAI and OAI on mixed-, (100)-, and (111)-oriented 3D bulk perovskites. We found that the thermal-lamination process compromises the performance of PSCs and simultaneously drives the disappearance or transformation of smaller-*n* 2D perovskites phases toward larger-*n* phases. By comparing mixed-orientation films with those predominantly exhibiting (100) and (111) dominated orientations, we reveal orientation-dependent degradation behaviours of low-dimensional

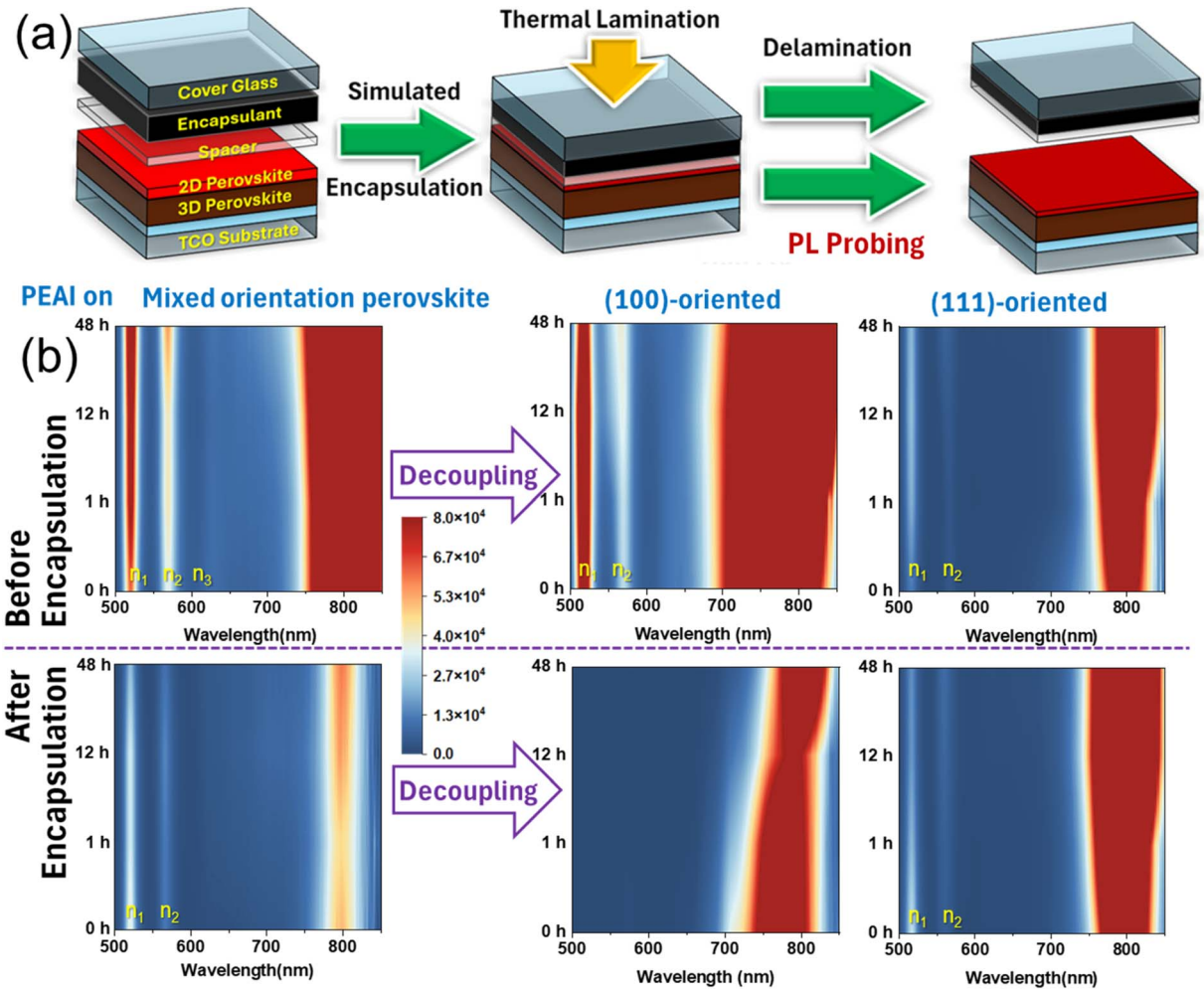

Fig. 1 (a) Schematic illustration of the preparation of hot-pressed encapsulated samples for characterization. (b) PL spectra of PEAI treated perovskite films before and after thermal-lamination (all contour plots share the same colour scale).

perovskite phases (n = 1, 2, 3) under thermal stress. Notably, (100)-oriented perovskites exhibited the most pronounced transformation of the 2D perovskite layer, whereas (111)-oriented structures exhibited minimal changes. These findings provide new insights into the structural evolution of perovskite interfaces during encapsulation and underscore the critical role of crystallographic orientation of perovskite in determining device stability, offering valuable guidance for the encapsulation of robust PSCs.

2 Results and discussion

A delamination approach was employed to systematically investigate the effects of thermal lamination on various 2D/3D perovskite heterostructure film samples (Fig. 1a). In this approach, a spacer layer was incorporated to form a multilayer structure consisting of Transparent Conductive Oxide (TCO) substrate/3D perovskite/2D perovskite/spacer/encapsulant/cover glass. Thermal lamination was applied to facilitate the even spreading of the encapsulant and to eliminate residual air between layers, replicating the practical encapsulation process for PSC fabrication (@95 °C, 0.5 mbar for 5 min and then 500 mbar for 5 min). Following lamination, the encapsulated sample can be separated as the spacer layer does not adhere to the underlying layers, enabling clean separation of the encapsulant without any environmental and mechanical damage. Considering the anisotropic nature of perovskite materials, these 2D/3D perovskite heterostructures were fabricated on (100)- and (111)-oriented 3D bulk perovskite films, respectively. Previous studies indicate that (100) and (111) facets exhibit distinct carrier transport and photocurrent behaviours, with (100) generally offering higher mobility.[21] The distribution of (100) facets within predominantly (111)-oriented films strongly affects optoelectronic performance and stability.[22] While a higher fraction of (100) orientation favours power conversion efficiency,[23] increasing (111) orientation enhances moisture resistance due to its denser atomic packing and limited exposure of reactive sites.[24,25] Notably, to get a pure (111)-oriented film we have incorporated a limited amount of Br in the film, which may compromise the perovskite stability. In this regard, if a pure (111)-oriented film without compositional change could be obtained, we would expect its stability to be at least comparable to, and possibly better than that of the current Br-containing (111)-oriented film. The orientation of the 3D perovskite films for 2D/3D construction is confirmed by X-ray diffraction (XRD, Fig. S1). The mixed-orientation 3D perovskite films exhibit multiple peaks, including (100) at 14.1°, (200) at 28.4°, and (111) at 24.5°, indicating the coexistence of various orientations. In contrast, (111)-oriented films show a dominant (111) peak with minor (100), (200), and PbI_2 peaks, while (100)-oriented films display prominent (100) and (200) peaks with no noticeable impurities. Subsequently, PEAI was deposited *via* spin-coating on 3D perovskite films with mixed, (100), and (111) out-of-plane orientations, constructing 2D/3D perovskite heterostructures.

After constructing the 2D/3D heterostructures, photoluminescence (PL) spectra of the films were immediately measured, followed by repeated measurements after 1 h, 24 h, and 48 h to obtain contour plots for a better understanding of the temporal evolution of the 2D/3D heterostructures (Fig. 1b). For the unencapsulated 2D/3D heterostructure based on a conventional perovskite film with mixed orientation, photoluminescence (PL) peaks assigned to 2D perovskite phases with different n values are observed, and their intensities decreased with increasing n value. After encapsulation, the intensities of these 2D-phase PL peaks decrease markedly, indicating disruption of the surface 2D passivation layer. Meanwhile, the PL peak of the 3D phase at ~800 nm also diminishes substantially, implying increased non-radiative recombination. To decouple facet-specific contributions, we fabricated (100)-oriented and (111)-oriented films and performed identical measurements with PEAI. The results show that after PEAI was deposited on the perovskite film surface, the (100)-oriented film more readily forms a 2D perovskite than the (111)-oriented film. However, the 2D perovskites constructed on the (100)-oriented film are unstable under thermal-lamination, with their PL signatures becoming barely detectable after encapsulation. In contrast, although 2D formation on the (111)-oriented film is less favourable, it is far less affected by the thermal-lamination process. After encapsulation, only a subtle kinetic reversal is observed, shifting from a slightly time-dependent increase to a weak decay, which suggests that the potential ingress of the bulky cations into the 3D perovskite is activated by a thermal lamination process. Overall, the 2D PL intensity shows no significant change when comparing measurements before and after encapsulation. Therefore, it is reasonable to infer that, for conventional mixed-orientation perovskite films, the post-encapsulation reduction in the PL signature of a PEA-based 2D perovskite arises predominantly from the loss of the 2D perovskite formed on (100) facets, whereas the residual 2D perovskites are mainly formed on (111) facets.

For the 2D/3D heterostructure constructed on a conventional mixed-orientation perovskite film, the encapsulation-induced changes lead to measurable variations in device performance. We compared the photovoltaic characteristics before and after encapsulation, using devices with a conventional p–i–n architecture of FTO/SnO_2/$FA_{0.9}Cs_{0.1}PbI_3$/PEAI/spiro-OMeTAD/Au, where PEAI was employed as a 2D passivation layer. As shown in Fig. 2, after encapsulation, a more pronounced performance loss in PEAI passivated devices is observed compared to the devices prepared without PEAI. Specifically, the power conversion efficiency (PCE) decreased by 6.55%, the open-circuit

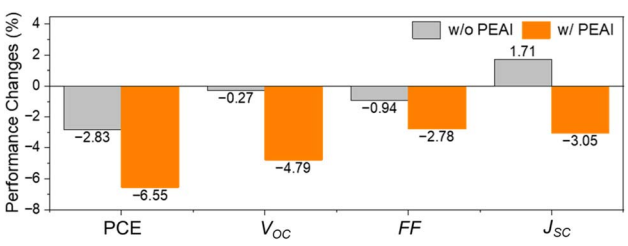

Fig. 2 Relative performance changes of PSCs prepared with mixed orientation perovskites before and after thermal-lamination.

voltage (V_{OC}) by 4.79%, the fill factor (FF) by 2.78%, and the current short-circuit density (J_{SC}) by 3.05% (full data provided in Fig. S2). In contrast, the PEAI-free devices exhibited relatively minor changes in performance, with PCE, FF, and V_{OC} decreasing by 2.83%, 0.27%, and 0.94%, respectively, while J_{SC} showed a slight increase of 1.71%. Such a modest rise in J_{SC} is likely associated with thermally induced, thermomechanical-stress-related structural relaxation occurring during the heating and encapsulation processes.[26,27] Meanwhile, morphology changes of the PEAI-based 2D/3D heterostructure before and after encapsulation can also be identified by SEM measurements (Fig. S3), whereas unpassivated 3D perovskite films exhibit no discernible encapsulation-induced changes (Fig. S4).[28] These observations indicate that encapsulation-driven materials change in the 2D/3D heterostructure identified by PL measurements is coupled with morphology changes, such as increased surface roughness (Fig. S5). And the combined encapsulation-driven reconstruction disrupts the optimized state of the original 2D passivation, thereby being responsible for the observed performance degradation.[29]

Furthermore, we extended the study to a broader set of passivation agents, probing their corresponding 2D/3D heterostructures formed on different facets and how they evolve upon encapsulation. By increasing the alkyl chain length from PEA (two carbons) to PPA (three) and PBA (four), larger bulky cations can be obtained.[28,29] The corresponding iodides of PPAI and PBAI are then deposited onto (100)- and (111)-oriented 3D perovskite surfaces. The temporal evolution of their PL spectra before and after encapsulation is shown in Fig. 3a. For both PPAI and PBAI samples without applying encapsulation, the PL peaks associated with smaller-n 2D phases decrease markedly with extended storage time, whereas those associated with larger-n 2D phases become stronger. This inverse trend suggests that the low-dimensional perovskite initially present in the 2D/3D heterostructure gradually turned into higher-dimensional perovskite, which is also known as invasive passivation.[13] This could be possibly because of bulky cations diffusing into the 3D lattice, thereby allowing more layers to be present in between them. Although this phenomenon can also be observed on both (100)- and (111)-oriented perovskites, the overall intensity of PL

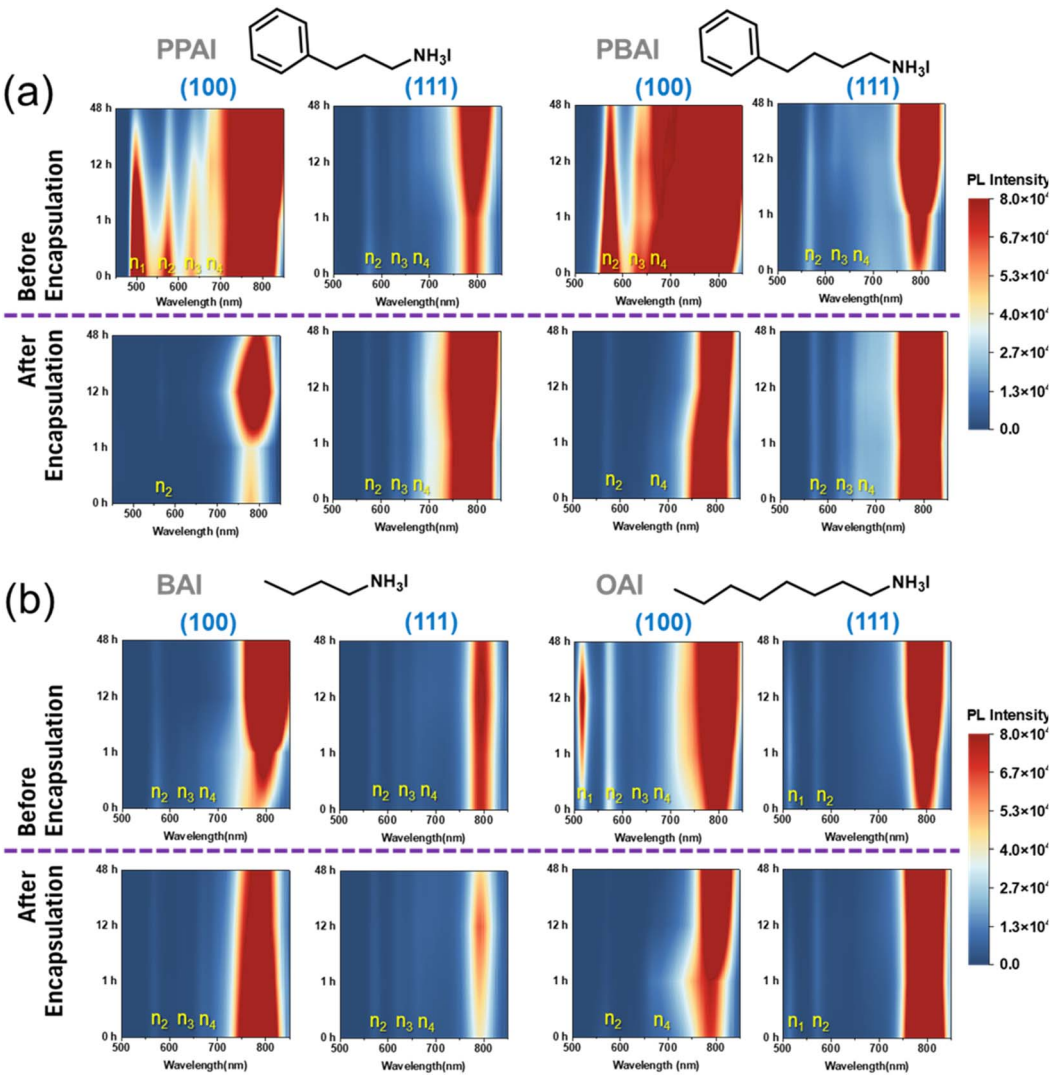

Fig. 3 PL spectra of perovskite films before and after thermal lamination: (a) PAAI- and PBAI-treated films and (b) BAI- and OAI-treated films.

emission on the (111)-oriented perovskite is still much weaker than that on the (100)-oriented perovskite, which is consistent with the PEAI case shown in Fig. 1. For both PPAI and PBAI samples with encapsulation applied, their PL spectra are much more stable with extended storage time. And at 0 h, their smaller-*n* 2D phases are less evident and larger-*n* 2D phases are enhanced compared to the unencapsulated counterparts at 48 h (Fig. S6), which suggests that the conversion of smaller-*n* 2D perovskites into larger-*n* 2D perovskites has been accelerated by the thermal lamination process during encapsulation. This is possibly because the thermal lamination supplies sufficient energy that drives the redistribution of the bulky cations, thereby yielding a more stable 2D/3D heterostructure after encapsulation. Notably, for both PPAI and PBAI samples on the (100)-oriented perovskite, the PL peaks in the 2D region are almost bleached after encapsulation, whereas for the (111)-oriented sample, the 2D signatures are largely retained, indicating that the 2D/3D heterostructure formed on the (111)-oriented perovskite is more stable under encapsulation. Although this phenomenon is observed on both (100)- and (111)-oriented perovskites, the overall intensity of the PL peak on the (111)-oriented perovskite is still much smaller than that on the (100)-oriented perovskite, which is consistent with PEAI. For the 2D/3D heterostructure formed on the (100)-oriented perovskite, the PL peaks in the 2D region are almost bleached after encapsulation, whereas for the (111)-oriented sample, the 2D signatures are largely retained. Notably, the 2D invasion behaviour is no longer observed after encapsulation, while the 2D peak in the larger-*n* region (650–750 nm) becomes stronger and more stable. We speculate that thermal lamination supplies sufficient energy that drives the redistribution of the bulky cations, thereby yielding a more stable 2D/3D heterostructure.

We also studied the 2D bulky cations without aromatic rings, as BAI and OAI are also widely used for 2D passivation in perovskite solar cells.[30–32] As shown in Fig. 3b, on the (100)-oriented perovskite, the PL intensity of BAI and OAI treated samples in the 2D perovskite region is weaker than that of the PEAI-, PPAI- and PBAI-treated samples; whilst on the (111)-oriented perovskite, their PL intensity in the 2D region is comparable. After encapsulation, the 2D PL peaks on the (100)-oriented perovskite are markedly weakened, whereas those formed on the (111)-oriented perovskite show much smaller changes, consistent with the trends observed previously for the PEAI-, PBAI- and PPAI-treated samples. From the above PL probing results, it is evident that 2D perovskite passivation layers form more easily on (100)-oriented perovskites than on their (111)-oriented counterparts irrespective of the passivating cation, but the 2D layers formed on (100)-oriented perovskites are unstable under the thermal-lamination conditions during encapsulation. In contrast, 2D perovskite passivation layers formed on (111)-oriented perovskites exhibit much greater tolerance to the encapsulation process.

To further elucidate the above observations and understand the formation and evolution of the 2D/3D heterostructures, we carried out density functional theory (DFT) calculations to examine the kinetics of 2D perovskite formation on (100)- and (111)-oriented 3D perovskite surfaces. As shown in Fig. 4, lattice models of $FAPbI_3$ with (100) and (111) orientations are first constructed. Because the formation of a 2D perovskite relies on the 3D framework supplying PbI_6 octahedra as the inorganic core, we calculated the formation energies for both the original 3D structure and the structure in which the surface PbI_6 octahedra are exfoliated. The exfoliated PbI_6 octahedra can serve as the core of a 2D perovskite with $n = 1$. By comparing the formation energies, it is found that the exfoliation energy of the surface PbI_6 octahedra requires 1.24 eV on the (100) orientation, and 1.63 eV on the (111) orientation. Therefore, the 2D perovskite can be formed more easily on (100)-oriented surfaces than on the (111) counterparts, which well explained our observation. Furthermore, we also calculated the structure with two layers of PbI_6 octahedra exfoliated. The formation of an $n = 2$ 2D perovskite on the (111)-oriented surface proceeds *via* a two-step pathway (Fig. S7). Specifically, surface PbI_6 octahedra first detach while largely retaining their original orientation, requiring an energy input of 0.7 eV. Subsequently, exfoliation of

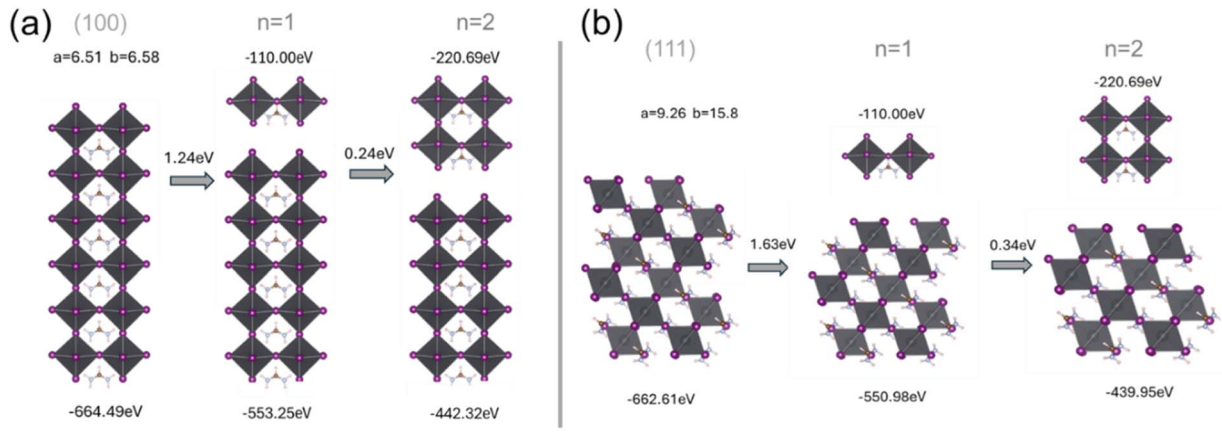

Fig. 4 (a) Schematic illustration of 2D perovskite formation on the (100) facet. (b) Schematic illustration of 2D perovskite formation on the (111) facet.

a second PbI_6 octahedral layer together with the already detached first layer releases 0.36 eV, resulting in a net energy cost of 0.34 eV for $n = 2$ formation on the (111)-oriented surface. The results indicate that additional energy inputs of 0.24 and 0.34 eV are required for the (100)- and (111)-oriented surfaces, respectively, to exfoliate a second PbI_6 octahedral layer in addition to the already detached first layer, thereby forming the inorganic framework of an $n = 2$ 2D perovskite. Obviously, the second exfoliation step requires much less energy than the first one, indicating that it is energetically more favourable to convert the existing smaller-n 2D perovskite into larger-n 2D perovskite phases. Based on the above calculations, it is reasonable to predict that direct formation of a larger-n 2D perovskite inorganic core from the 3D perovskite requires more energy than the formation of a smaller-n core. This is consistent with our experimental observation that spin-coating bulky organic halides on 3D perovskite films preferentially produces smaller-n 2D perovskites, while the extra energy provided by the thermal lamination step promotes their conversion into larger-n 2D perovskites and ultimately approaching quasi-3D perovskites. Moreover, the higher exfoliation energy of the (111)-oriented surface further leads to larger energy barrier for the conversion of 2D perovskite phases, which explains its superior resilience to encapsulation-induced structural changes compared with the (100)-oriented surface as observed from our PL probing results.

3 Conclusions

In summary, it is demonstrated that the 2D/3D heterostructure in perovskite solar cells can be significantly affected by the thermal-lamination applied to the device during the encapsulation process. Encapsulation can substantially disrupt the 2D perovskite passivation layer, leading to a noticeable deterioration in device performance. In particular, the 2D perovskite formed on (100)-oriented surfaces is more severely damaged by encapsulation, whereas the 2D layer formed on (111)-oriented surfaces is considerably more stable, though it is relatively more difficult to form. Furthermore, the thermal lamination process accelerates the conversion of smaller-n 2D perovskites into larger-n 2D perovskites, thereby promoting the formation of higher-dimensional perovskite structures. These findings provide valuable insights into the mechanisms governing the evolution of 2D/3D heterostructures and will benefit the development of reliable encapsulation strategies for perovskite-based photovoltaic devices and broader optoelectronic applications.

Conflicts of interest

The authors declare no conflict of interest.

Data availability

The data supporting this article have been included as part of the supplementary information (SI). Supplementary information: Fig. S1–S7. See DOI: https://doi.org/10.1039/d6el00069j.

Acknowledgements

X. L.'s experimental work was supported by the National Natural Science Foundation of China (No. 62204211). M. Z. acknowledges the Australian Research Council (ARC) Discovery Early Career Researcher Award Fellowship (DE230100163). X. H. acknowledges the ARC Future Fellowship (FT190100756).

References

1 M. A. Green, E. D. Dunlop, M. Yoshita, *et al.*, "Solar Cell Efficiency Tables (Version 66)", *Prog. Photovoltaics Res. Appl.*, 2025, **33**(7), 795–810, DOI: 10.1002/pip.3919.
2 T. Wu, R. Zhao, D. Jia, *et al.*, "In-depth Understanding the Effect of Electron-Withdrawing/-Donating Groups on the Interfacial Carrier Dynamics in Naphthalimide-Treated Perovskite Solar Cells", *J. Energy Chem.*, 2023, **77**, 514–520, DOI: 10.1016/j.jechem.2022.11.030.
3 J. Liu, M. Zhang, X. Sun, *et al.*, "Scalable Fabrication of Methylammonium-Free Wide-Bandgap Perovskite Solar Cells by Blade Coating in Ambient Air", *Nano-Micro Lett.*, 2025, **17**(1), 318, DOI: 10.1007/s40820-025-01838-6.
4 T. Hou, M. Zhang, X. Sun, *et al.*, "Methylammonium-Free Ink for Low-Temperature Crystallization of α-$FAPbI_3$ Perovskite", *Adv. Energy Mater.*, 2024, **14**(30), 2400932, DOI: 10.1002/aenm.202400932.
5 T. Wu, M. Zhang, X. Gao, *et al.*, "Self-Assembled Monolayers for Perovskite Solar Cells: Molecular Design and Chemical Synthesis", *ACS Nano*, 2025, **19**(7), 6234–6251, DOI: 10.1021/acsnano.5c05601.
6 J. Wang, S. Hu, Z. Chen, *et al.*, "Exposing Binding-Favourable Facets of Perovskites for Tandem Solar Cells", *Energy Environ. Sci.*, 2025, **18**, 7680–7694, DOI: 10.1039/d5ee02462e.
7 H. Kim, S.-M. Yoo, B. Ding, *et al.*, "Shallow-Level Defect Passivation by 6H Perovskite Polytype for Highly Efficient and Stable Perovskite Solar Cells", *Nat. Commun.*, 2024, **15**(1), 5632, DOI: 10.1038/s41467-024-50016-6.
8 Y. Lin, Y. Fang, J. Zhao, *et al.*, "Unveiling the Operation Mechanism of Layered Perovskite Solar Cells", *Nat. Commun.*, 2019, **10**(1), 1008, DOI: 10.1038/s41467-019-08958-9.
9 Q. Jiang, Y. Zhao, X. Zhang, *et al.*, "Surface Passivation of Perovskite Film for Efficient Solar Cells", *Nat. Photonics*, 2019, **13**(7), 460–466, DOI: 10.1038/s41566-019-0398-2.
10 A. B. Kaplan, Q. C. Burlingame, M. R. Ivancevic, *et al.*, "Understanding the Structural Dynamics of 2D/3D Perovskite Interfaces", *ACS Appl. Mater. Interfaces*, 2025, **17**(11), 16963–16969, DOI: 10.1021/acsami.5c02680.
11 S. Sidhik, Y. Wang, M. De Siena, *et al.*, "Deterministic Fabrication of 3D/2D Perovskite Bilayer Stacks for Durable and Efficient Solar Cells", *Science*, 2022, **377**(6613), 1425–1430, DOI: 10.1126/science.abq7652.
12 C. Liu, Y. Yang, J. D. Fletcher, *et al.*, "Cation Interdiffusion Control for 2D/3D Heterostructure Formation and Stabilization in Inorganic Perovskite Solar Modules", *Nat. Energy*, 2025, **10**(8), 981–990, DOI: 10.1038/s41560-025-01817-6.

13 S. M. Park, M. Wei, J. Xu, *et al.*, "Engineering Ligand Reactivity Enables High-Temperature Operation of Stable Perovskite Solar Cells", *Science*, 2023, **381**(6654), 209–215, DOI: 10.1126/science.adi4107.

14 E. A. Gaulding, A. E. Louks, M. Yang, *et al.*, "Package Development for Reliability Testing of Perovskites", *ACS Energy Lett.*, 2022, **7**(8), 2641–2645, DOI: 10.1021/acsenergylett.2c01168.

15 L. Shi, T. L. Young, J. Kim, *et al.*, "Accelerated Lifetime Testing of Organic–Inorganic Perovskite Solar Cells Encapsulated by Polyisobutylene", *ACS Appl. Mater. Interfaces*, 2017, **9**(30), 25073–25081, DOI: 10.1021/acsami.7b07625.

16 L. Shi, M. P. Bucknall, T. L. Young, *et al.*, "Gas Chromatography–Mass Spectrometry Analyses of Encapsulated Stable Perovskite Solar Cells", *Science*, 2020, **368**(6497), eaba2412, DOI: 10.1126/science.aba2412.

17 Y. Zhang, X. Liu, X. Sun, *et al.*, "Barrier Strategy for Strain-Free Encapsulation of Perovskite Solar Cells", *J. Phys. Chem. Lett.*, 2023, **14**(48), 10754–10761, DOI: 10.1021/acs.jpclett.3c02636.

18 W. Yang, Y. Zhang, C. Xiao, *et al.*, "A Review of Encapsulation Methods and Geometric Improvements of Perovskite Solar Cells and Modules for Mass Production and Commercialization", *Nano Mater. Sci.*, 2025, **7**(6), 790–809, DOI: 10.1016/j.nanoms.2025.02.005.

19 Q.-Q. Chu, Z. Sun, D. Wang, *et al.*, "Encapsulation: The Path to Commercialization of Stable Perovskite Solar Cells", *Matter*, 2023, **6**(11), 3838–3863, DOI: 10.1016/j.matt.2023.08.016.

20 F. Toniolo, H. Bristow, M. Babics, *et al.*, "Efficient and Reliable Encapsulation for Perovskite/Silicon Tandem Solar Modules", *Nanoscale*, 2023, **15**(42), 16984–16991, DOI: 10.1039/d2nr06873g.

21 C. Ma, M.-C. Kang, S.-H. Lee, *et al.*, "Photovoltaically Top-Performing Perovskite Crystal Facets", *Joule*, 2022, **6**(11), 2626–2643, DOI: 10.1016/j.joule.2022.09.012.

22 X. Zheng, Y. Hou, C. Bao, *et al.*, "Managing Grains and Interfaces via Ligand Anchoring Enables 22.3%-Efficiency Inverted Perovskite Solar Cells", *Nat. Energy*, 2020, **5**(2), 131–140, DOI: 10.1038/s41560-019-0538-4.

23 X. Li, S. Gao, X. Wu, *et al.*, "Bifunctional Ligand-Induced Preferred Crystal Orientation Enables Highly Efficient Perovskite Solar Cells", *Joule*, 2024, **8**(11), 3169–3185, DOI: 10.1016/j.joule.2024.07.009.

24 C. Ma, F. T. Eickemeyer, S.-H. Lee, *et al.*, "Unveiling Facet-Dependent Degradation and Facet Engineering for Stable Perovskite Solar Cells", *Science*, 2023, **379**(6628), 173–178, DOI: 10.1126/science.adf3349.

25 B. Zhou, P. Zhao, J. Guo, *et al.*, "Unveiling the Importance of Nondominant Facets in (111)-Dominated Perovskite Films", *ACS Appl. Mater. Interfaces*, 2025, **17**(15), 22715–22726, DOI: 10.1021/acsami.5c04126.

26 L. Wu, S. Hu, F. Yang, *et al.*, "Resilience pathways for halide perovskite photovoltaics under temperature cycling", *Nat. Rev. Mater.*, 2025, **10**, 536–549, DOI: 10.1038/s41578-025-00781-7.

27 S. M. Mousavi, H. D. Shirazi, R. Ranta, *et al.*, "Addressing the Efficiency Loss and Degradation of Triple Cation Perovskite Solar Cells via Integrated Light Managing Encapsulation", *Mater. Today Energy*, 2024, **46**, 101707, DOI: 10.1016/j.mtener.2024.101707.

28 F. Zhang, S. Ye, H. Zhang, *et al.*, "Comprehensive Passivation Strategy for Achieving Inverted Perovskite Solar Cells with Efficiency Exceeding 23% by Trap Passivation and Ion Constraint", *Nano Energy*, 2021, **89**, 106370, DOI: 10.1016/j.nanoen.2021.106370.

29 S. Tan, M.-C. Shih, Y. Lu, *et al.*, "Spontaneous Formation of Robust Two-Dimensional Perovskite Phases", *Science*, 2025, **388**(6747), 639–645, DOI: 10.1126/science.adr1334.

30 H. Kim, S.-U. Lee, D. Y. Lee, *et al.*, "Optimal Interfacial Engineering with Different Length of Alkylammonium Halide for Efficient and Stable Perovskite Solar Cells", *Adv. Energy Mater.*, 2019, **9**(47), 1902740, DOI: 10.1002/aenm.201902740.

31 S. Xiong, F. Tian, F. Wang, *et al.*, "Reducing Nonradiative Recombination for Highly Efficient Inverted Perovskite Solar Cells via a Synergistic Bimolecular Interface", *Nat. Commun.*, 2024, **15**(1), 5607, DOI: 10.1038/s41467-024-50019-3.

32 H. Wang, F. Ye, J. Liang, *et al.*, "Pre-Annealing Treatment for High-Efficiency Perovskite Solar Cells via Sequential Deposition", *Joule*, 2022, **6**(12), 2869–2884, DOI: 10.1016/j.joule.2022.10.00.